The effects of cooling rate on particle rearrangement statistics: Rapidly cooled glasses are more ductile and less reversible

Meng Fan,[1,2] Minglei Wang,[1,2] Kai Zhang,[3] Yanhui Liu,[1,2] Jan Schroers,[1,2] Mark D. Shattuck,[4,1] and Corey S. O'Hern[1,2,5,6]

[1]*Department of Mechanical Engineering and Materials Science, Yale University, New Haven, Connecticut, 06520, USA*
[2]*Center for Research on Interface Structures and Phenomena, Yale University, New Haven, Connecticut, 06520, USA*
[3]*Department of Chemical Engineering, Columbia University, New York, New York 10027, USA*
[4]*Department of Physics and Benjamin Levich Institute, The City College of the City University of New York, New York, New York, 10031, USA*
[5]*Department of Physics, Yale University, New Haven, Connecticut, 06520, USA*
[6]*Department of Applied Physics, Yale University, New Haven, Connecticut, 06520, USA*

(Dated: July 15, 2016)

Amorphous solids, such as metallic, polymeric, and colloidal glasses, display complex spatiotemporal response to applied deformations. In contrast to crystalline solids, during loading, amorphous solids exhibit a smooth crossover from elastic response to plastic flow. In this study, we investigate the mechanical response of binary Lennard-Jones glasses to athermal, quasistatic pure shear as a function of the cooling rate used to prepare them. We find several key results concerning the connection between strain-induced particle rearrangements and mechanical response. We show that more rapidly cooled glasses undergo more frequent and larger particle rearrangements than slowly cooled glasses. We find that the ratio of the shear to bulk moduli decreases with increasing cooling rate, which suggests that more rapidly cooled glasses are more ductile than slowly cooled samples. In addition, we characterized the degree of reversibility of particle motion during cyclic shear. We find that irreversible particle motion occurs even in the putative linear regime of stress versus strain. However, slowly cooled glasses, which undergo smaller rearrangements, are more reversible under cyclic shear than rapidly cooled glasses. Thus, we show that more ductile glasses are also less reversible.

PACS numbers: 62.20.-x, 63.50.Lm 64.70.kj 64.70.pe

arXiv:1607.04221v1 [cond-mat.soft] 14 Jul 2016

Amorphous solids, including metallic, polymeric, and colloidal glasses, possess complex mechanical response to applied deformations, such as plastic flow [1–4], strain localization [5–9], creep flow [7, 10, 11], and fracture [12–14]. In crystalline materials, topological defects reflecting the symmetry of the crystalline phase govern the response to applied deformations. In amorphous solids without long-range positional order, it is more difficult to detect and predict changes from elastic response to irreversible behavior [8, 15], such as yielding [16, 17] and flow [4, 18]. The typical response of the deviatoric stress to an applied (pure) shear strain for amorphous solids is depicted in Fig. 1 (a). The average stress increases roughly linearly with strain for small strains, indicating a putative elastic regime. At larger strains, the stress response softens and becomes anelastic, but it continues to increase with strain. For larger strains (*i.e.* near $\gamma \sim 0.05$), the shear stress reaches a peak (whose height depends on the thermal history of the glass) and then begins to decrease until it plateaus at a steady state value in the plastic flow regime [2, 18]. (For this system, we employed boundary conditions that prevent fracture.)

Several recent studies have suggested that amorphous solids do not possess a truly elastic response regime [6, 7, 9, 16, 19–21]. For example, both a sublinear increase of the average stress with strain (left inset to Fig. 1 (a)) and rapid drops in stress over narrow strain intervals (right inset to Fig. 1 (a)) have been observed at strains below the nominal yield strain of 2% [16, 19, 21]. The rapid drops in stress are caused by particle rearrangements (*e.g.* in Fig. 1 (b)), which are often referred to as shear transformation zones [1, 22, 23]. We will show below how the frequency and size of particle rearrangements determine the mechanical response of amorphous solids.

In this article, we build a conceptual framework for the mechanical response of amorphous solids by exploring the potential energy landscape and particle rearrangement statistics of binary Lennard-Jones glasses during athermal, quasistatic pure shear. The initial glasses are prepared over a wide range of cooling rates. The cooling rate determines the fictive temperature, which defines the average energy of the glass in the potential energy landscape [25]. The fictive temperature significantly affects mechanical properties, such as ductility [14, 26], shear band formation [27], and the stress-strain relation [2, 28]. Our key result is that more rapidly cooled glasses possess more frequent and larger potential energy drops during applied shear strain compared to more slowly cooled glasses. As a result, the ensemble-averaged (metabasin) curvature of the energy landscape is much smaller for rapidly cooled glasses. We connect the statistics of particle rearrangements to whether amorphous solids exhibit brittle or ductile mechanical response and characterize the degree of irreversibility of particle rearrangements in

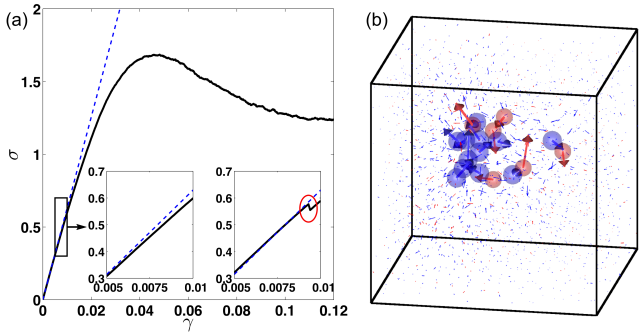

Figure 1: (a) von Mises stress σ versus strain γ (solid line) from simulations of a binary Lennard-Jones glass (prepared at cooling rate $R_c = 10^{-3}$) with $N = 2000$ spheres undergoing athermal, quasistatic pure shear averaged over 500 samples. Periodic boundary conditions are employed in the simulations, which prevent fracture during loading. The affine stress versus strain obtained in the $\gamma \to 0$ limit is given by the dashed line. The left inset provides a close-up of the ensemble-averaged $\sigma(\gamma)$, which highlights the deviation from linear behavior in the range $\gamma = 0.005$ to 0.01. The right inset gives $\sigma(\gamma)$ for a single sample over the same small strain interval. The circled stress drop indicates the particle rearrangement event in (b). The vectors (which have been scaled by a factor of 15) indicate the particle displacements that caused the stress drop. The participation number [24] of this event is roughly 18. Blue and red spheres indicate the large and small particles, respectively, with the largest displacements.

response to shear reversal. We find that more rapidly cooled glasses are more ductile and irreversible compared to slowly cooled glasses.

We performed constant number, pressure, and temperature (NPT) molecular dynamics (MD) simulations of binary Lennard-Jones mixtures containing 80% large and 20% small spherical particles by number (both with mass m) in a cubic box with volume V and periodic boundary conditions. The particles interact pairwise via the Kob-Andersen, shifted-force potential, $u(r_{ij}) = 4\epsilon_{ij}[(\sigma_{ij}/r_{ij})^{12} - (\sigma_{ij}/r_{ij})^6]$, where r_{ij} is the separation between particles i and j, $u(r_{ij}) = 0$ for $r_{ij} > 2.5\sigma_{ij}$, and the energy and length parameters are given by $\epsilon_{AA} = 1.0$, $\epsilon_{BB} = 0.5$, $\epsilon_{AB} = 1.5$, $\sigma_{AA} = 1.0$, $\sigma_{BB} = 0.88$, and $\sigma_{AB} = 0.8$ [29]. Energy, temperature, pressure, and time scales are expressed in units of ϵ_{AA}, ϵ_{AA}/k_B, $\epsilon_{AA}/\sigma_{AA}^3$, and $\sigma_{AA}\sqrt{m/\epsilon_{AA}}$, respectively, where k_B is Boltzmann's constant [30].

We first equilibrate systems in the liquid regime at constant temperature $T_0 = 0.6$ and pressure $P = 0.025$ using a Nosé-Hoover thermostat and barostat, a second-order simplectic integration scheme [31, 32], and time step $\Delta t = 10^{-3}$. We cool systems into a glassy state at zero temperature using a linear cooling ramp, $T(t) = T_0 - R_c t$ over a range of cooling rates from $R_c = 10^{-2}$ to 10^{-5}, all of which are above the critical cooling rate. Thus, all of the zero-temperature samples are disordered. We then apply athermal, quasistatic pure shear at fixed pressure. (See an expanded discussion of the methods in the Supplemental Material.) To do this, we expand the box length and move all particles affinely in the x-direction by a small strain increment $d\gamma_x = d\gamma = 10^{-4}$ and compress the box length and move all particles affinely in the y-direction by the same strain increment $d\gamma_y = -d\gamma$. Following the applied pure shear strain, we minimize the total enthalpy of the system $H = \mathcal{U} + PV$ at fixed pressure $P = 10^{-8}$, where $\mathcal{U}$ is the total potential energy. We successively apply pure strain increments $d\gamma$ and minimize the enthalpy at fixed pressure after each increment to a total strain γ. We studied systems with $N = 250$, 500, 1000, and 2000 particles to assess finite size effects.

We developed a method to unambiguously determine if a particle rearrangement occurs with an accuracy on the order of numerical precision, which allows us to detect rearrangements with sizes ranging over more than seven orders of magnitude. To identify particle rearrangement events, at each strain γ we compare the total potential energy per particle $U(\gamma) = \mathcal{U}(\gamma)/N$ from simulations undergoing forward shear to the potential energy per particle $U'(\gamma)$ obtained by first a forward shear step from strain γ to $\gamma + d\gamma$ (and enthalpy minimization) followed by a backward shear step from $\gamma + d\gamma$ back to γ (and enthalpy minimization). We find that the distribution of the magnitudes of the energy differences $|\Delta U(\gamma)| = |U(\gamma) - U'(\gamma)|$ is bimodal with peaks near 10^{-14} corresponding to numerical error and 10^{-3} corresponding to distinct particle rearrangements. Thus, it is straightforward to identify particle rearrangements as those with $|\Delta U| > U_t$, where the threshold $U_t = 10^{-10}$ clearly distinguishes numerical error from particle rearrangements. (See Supplemental Material.) We denote the total number of rearrangements in the strain interval 0 to γ as $N_r(\gamma)$. In addition, we calculate the total energy lost after each rearrangement $i = 1, \ldots, N_r(\gamma)$ over the strain interval γ: $U_{\rm loss} = \sum_{i=1}^{N_r(\gamma)} |\Delta U(\gamma_i)|$, where γ_i indicate the strains at which rearrangements occur.

In Fig. 2 (a) and (b), we plot the frequency of rearrangements $dN_r/d\gamma$ and energy loss per rearrangement $dU_{\rm loss}/dN_r$ as a function of strain. Both the frequency and energy loss increase with strain for small strains ($\gamma < 0.05$ for $dN_r/d\gamma$ and $\gamma < 0.08$ for $dU_{\rm loss}/dN_r$) and then reach plateau values that are independent of strain. Both quantities are sensitive to cooling rate in the small strain regime: glasses quenched using more rapid cooling rates (*i.e.* $R = 10^{-2}$) incur more and larger particle rearrangements. For more slowly cooled glasses (*i.e.* $R = 10^{-5}$), the systems only begin losing energy (as measured from $dU_{\rm loss}/d\gamma$) beyond a characteristic strain $\gamma_c \approx 0.02$. In contrast, for rapidly cooled glasses, the energy loss is roughly proportional to strain for $\gamma < 0.06$. At large strains $\gamma > 0.06$, $dU_{\rm loss}/d\gamma$ becomes independent of cooling rate and strain. Further, we find that $dU_{\rm loss}/d\gamma$, which is the product of $dN_r/d\gamma$ and $dU_{\rm loss}/dN_r$, is roughly independent of system size over the range of N we consider.

The potential energy landscape, which in the case of

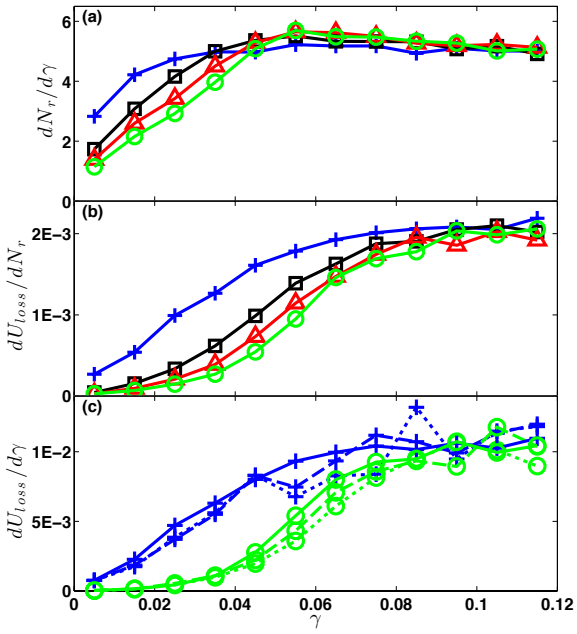

Figure 2: (a) Particle rearrangement frequency $dN_r/d\gamma$, (b) mean energy drop per rearrangement $dU_{\rm loss}/dN_r$, and (c) the product of (a) and (b), the energy drop per strain $dU_{\rm loss}/d\gamma$, as a function of strain for several cooling rates $R_c = 10^{-2}$ (crosses), 10^{-3} (squares), 10^{-4} (triangles), and 10^{-5} (circles) used to prepare the binary Lennard-Jones glasses. In (a) and (b), the curves are obtained by averaging over 500 samples containing $N = 2000$ particles. In (c), we show $dU_{\rm loss}/d\gamma$ for three system sizes: $N = 2000$ (solid lines), 1000 (dashed lines), and 500 (dotted lines).

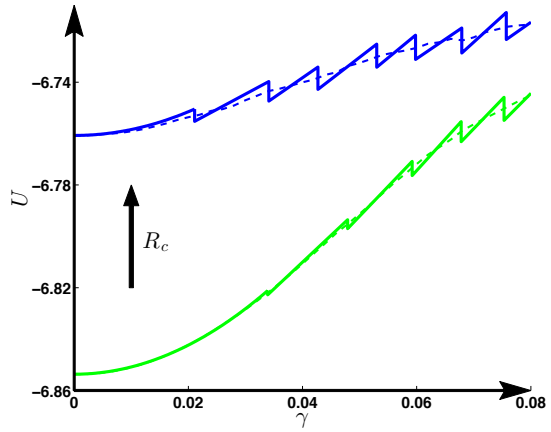

Figure 3: Total potential energy per particle U versus strain γ for binary Lennard-Jones glasses containing $N = 250$ particles prepared using cooling rates $R_c = 10^{-2}$ (top) and 10^{-5} (bottom) and then subjected to athermal, quasistatic pure shear. The solid and dashed lines indicate single-configuration (with average particle rearrangement statistics; see Supplemental Material) and ensemble-averaged $U(\gamma)$, respectively.

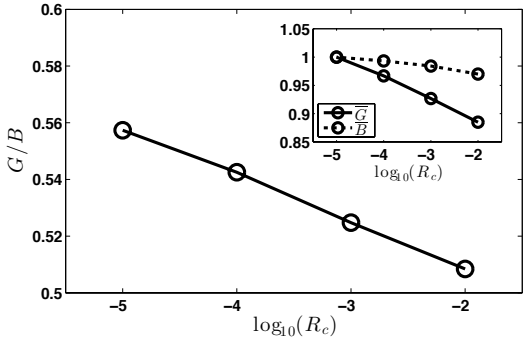

Figure 4: The ratio of the shear to bulk modulus G/B as a function of the cooling rate R_c used to prepare the binary Lennard-Jones glasses. The inset shows the shear $\overline{G}$ and bulk moduli $\overline{B}$ separately as a function of R_c, both of which have been normalized to 1 at $R_c = 10^{-5}$.

pure shear is a function of the $3N$ particle coordinates and strain γ, can provide key insights into the structure of configuration space and mechanical behavior of glassy materials [25, 33]. For example, recent studies have identified hierarchical sub- and metabasins in the energy landscape of supercooled liquids and glasses [18, 25, 34] and studied the disappearance of energy minima and resulting particle rearrangements as a function of applied strain [24, 25, 35]. In Fig. 3, we show the total potential energy per particle U versus strain γ for a single configuration (with average particle rearrangement statistics), as well as $U(\gamma)$ averaged over 500 configurations, for two cooling rates ($R_c = 10^{-5}$ and 10^{-2}). For the more rapidly cooled glass, the energy drops are relatively large and frequent. Rearrangements are frequent because there is an abundance of nearby minima in the potential energy landscape as a function of strain for rapidly cooled glasses [33]. In addition, the large and frequent energy drops give rise to small metabasin curvature of the ensemble-averaged energy landscape.

In contrast, for slowly cooled glasses, we find that the energy drops are smaller and more rare, which implies that when systems are deeper in the energy landscape, energy minima are further separated as a function of strain and the curvatures of the energy metabasins are larger. Thus, these results provide evidence that the curvatures of the metabasins in the potential energy landscape decrease with increasing cooling rate [2, 36]. In addition, our results are consistent with prior results, which show that the yield stress (or the ensemble-averaged $dU/d\gamma$) increases with decreasing cooling rate [2, 28].

We next connect the statistics of the potential energy landscape to micro- and macro-scale mechanical properties of amorphous solids. As shown in Fig. 3, more rapidly cooled glasses undergo larger and more frequent particle rearrangements. We argue that larger and more frequent particle rearrangements help reduce stress accumulation during deformation and hence prevent catastrophic brittle failure [27, 37, 38]. This suggests that

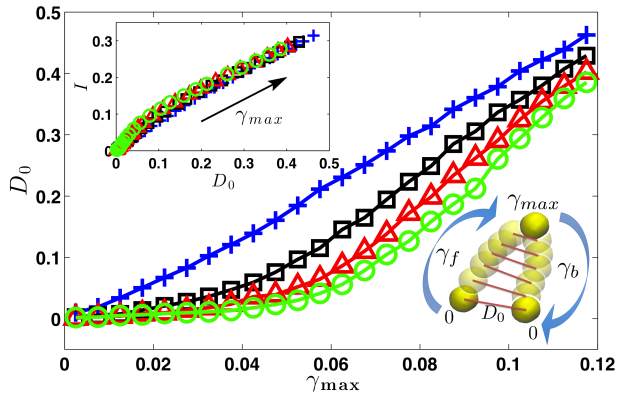

Figure 5: Measurement D_0 of the degree to which a system deviates from the original unsheared configuration after undergoing a single athermal quasistatic pure shear cycle with strain amplitude $\gamma_{\max}$ for several cooling rates: $R_c = 10^{-2}$ (crosses), 10^{-3} (squares), 10^{-4} (triangles), and 10^{-5} (circles). The curves were averaged over 96 samples with $N = 2000$. The upper left inset shows that the two measures of irreversibility, D_0 and I, are positively correlated. The lower right inset shows a schematic of the trajectory of a single particle during forward shear from total strain 0 to $\gamma_{\max}$ and backward shear from total strain $\gamma_{\max}$ to 0. The bars connect the particle positions at corresponding strains during the trajectory, $\vec{R}(\gamma', 0)$ and $\vec{R}(\gamma_{max}, \gamma_{max} - \gamma')$. D_0 and I are related to the length of the lower bar and the average length over all bars, respectively.

more rapidly quenched glasses are more ductile than slowly quenched glasses [14]. To investigate this hypothesis, we measured the ratio of the shear to bulk modulus G/B (Fig. 4) as a function of cooling rate. (The moduli G and B were obtained from the slope of $\sigma(\gamma)$ for vanishingly small pure and compressive strains, respectively.) G/B is a material property that has been shown to correlate strongly with the ductility/brittleness of a material [14, 37, 39, 40]. We find that both G and B decrease with increasing cooling rate, but G decreases faster (inset to Fig. 4), and thus the ratio G/B, and brittleness, decrease with increasing R_c.

Whether a material is reversible or not under applied deformation is often inferred from the behavior of its stress-strain curve or other macroscopic measurements. For example, materials are typically deemed reversible in the regime where the stress-strain curve is linear, and irreversible in the regime where plastic flow occurs [41]. Reversibility has been studied experimentally using enthalpy [18] and strain recovery [19], elastostatic compression [16], nanoindentation [10], and quality factor measurements [42]. In simulations, reversibility has been studied using cyclic shear of model glasses [17, 43–46]. Though the large elastic region (*e.g.* the linear stress-strain region in Fig. 1) is typically considered reversible, recent measurements have been identified irreversible events and anelasticity on the micro-scale in this 'elastic' region [6, 7, 9, 16, 19–21].

An important, fundamental open challenge is to determine the onset [43, 44] of micro-scale irreversibility and understand its connection to irreversibility and plasticity on macroscopic scales. Above, we defined particle rearrangements as those that led to local irreversibility of the potential energy after a forward strain increment $d\gamma$, followed by a backward strain increment $-d\gamma$. We now characterize the reversibility of particle motion following *finite-sized* strains using two measures. First, we define a measure of "state" irreversibility as

$$D_0(\gamma) = |\vec{R}(0,0) - \vec{R}(\gamma,\gamma)|/N, \qquad (1)$$

where $\vec{R}(\gamma_f, \gamma_b)$ gives the particle coordinates after the system has been sheared forward by strain γ_f and backward by strain γ_b. D_0 characterizes the ability of a sheared system to return to the original, unsheared configuration. (See the lower right inset to Fig. 5.) In Eq. 1, $\vec{R}(0,0)$ gives the original, unsheared particle coordinates, and $\vec{R}(\gamma,\gamma)$ gives the particle coordinates of the system after it was sheared forward to strain γ and then sheared backward from strain γ to zero strain. During forward strain, the system undergoes $N_r(\gamma)$ particle rearrangements and during backward strain, the system undergoes a different set of $N_r(-\gamma)$ particle rearrangements. $D_0(\gamma) \sim 0$ indicates a type of reversible behavior, where most of the particles return to their original, unsheared positions after a strain cycle of amplitude γ. In contrast, $D_0 > 0$ implies irreversible behavior that grows in magnitude with increasing D_0. We also define a measure of "path" irreversibility,

$$I(\gamma) = \frac{1}{N}\sqrt{\frac{1}{\gamma}\int_0^{\gamma} |\vec{R}(\gamma',0) - \vec{R}(\gamma,\gamma-\gamma')|^2 d\gamma'}, \qquad (2)$$

which determines the average distance between the system configurations at corresponding strains during the forward and backward portions of the shear cycle. (See the lower right inset to Fig. 5.)

Even though shear cycles can occur with $I > 0$ and $D_0 = 0$, which implies that the system returns to the original, unsheared configuration at $\gamma = 0$ along different forward and backward shear paths [43], we find that the ensemble-averaged I becomes nonzero only when D_0 begins increasing from zero. Further, I and D_0 are strongly correlated as the amplitude $\gamma_{\max}$ of the shear cycle increases. (See the upper left inset in Fig. 5.) In Fig. 5, we plot $D_0(\gamma_{max})$ for several cooling rates. We find that slowly cooled glasses are nearly reversible over a finite range of strain (*i.e.* up to $\gamma_{\max} \sim \gamma_y = 0.05$), while $D_0 \sim A\gamma_{\max}$ (with slope A) for rapidly cooled glasses. For intermediate cooling rates, D_0 can be approximated as $D_0 \sim B(R_c)\gamma_{\max}$ for $\gamma_{\max} < \gamma_y(R_c)$ and $D_0 \sim A\gamma_{\max}$ for $\gamma_{\max} > \gamma_y(R_c)$. The slope $B(R_c)$ increases with cooling rate, and the crossover strain $\gamma_y(R_c)$ decreases with cooling rate. The upper inset to Fig. 5 shows that I and D_0 possess the same cooling rate dependence. More rapidly cooled glasses possess higher values of irreversibil-

ity because they undergo more frequent and larger rearrangements during shear (as shown in Fig. 3). In addition, we have shown that the path irreversibility I is strongly correlated with the energy loss per rearrangement $dU_{\rm loss}/dN_r$.

It is well known that non-affine particle motion and rearrangements control the mechanical properties of amorphous solids. In this study, we showed that the particle rearrangement statistics are sensitive to the cooling rate used to prepare zero-temperature glasses. Specifically, we identified distinct particle rearrangement events in binary Lennard-Jones glasses undergoing athermal, quasistatic pure shear. We measured the frequency of rearrangements and the size of the energy drops during rearrangements as a function of strain and the cooling rate used to prepare the glasses. We found that more rapidly cooled glasses undergo more frequent and larger energy drops, compared to more slowly cooled glasses. We also correlated the statistics of particle rearrangements to the ratio of the shear and bulk moduli and showed that more rapidly cooled glasses are more ductile than slowly cooled glasses. Finally, we characterized the degree of irreversibility of systems to cyclic shear and showed that slowly cooled glasses possess a finite range of strain where they appear nearly reversible (but are not truly reversible with $D_0 = I = 0$), whereas measures of irreversibility increase linearly with strain for rapidly cooled glasses. Thus, we showed that more ductile glasses are also more irreversible, and connected particle-scale rearrangement statistics to macroscopic mechanical response.

Acknowledgments

The authors acknowledge primary financial support from NSF MRSEC DMR-1119826 (K.Z.) and partial support from NSF Grant Nos. CMMI-1462439 (C.O. and M.F.) and CMMI-1463455 (M.S.). This work also benefited from the facilities and staff of the Yale University Faculty of Arts and Sciences High Performance Computing Center and the NSF (Grant No. CNS-0821132) that, in part, funded acquisition of the computational facilities.

[1] M. L. Falk and J. S. Langer, Physical Review E **57**, 7192 (1998).
[2] M. Utz, P. G. Debenedetti, and F. H. Stillinger, Physical Review Letters **84**, 1471 (2000).
[3] C. Maloney and A. Lemaitre, Physical Review Letters **93**, 016001 (2004).
[4] B. A. Sun, H. B. Yu, W. Jiao, H. Y. Bai, D. Q. Zhao, and W. H. Wang, Physical Review Letters **105**, 35501 (2010).
[5] F. Spaepen, Acta Metallurgica **25**, 407 (1977).
[6] P. Schall, D. A. Weitz, and F. Spaepen, Science **318**, 1895 (2007).
[7] J. Ju, D. Jang, A. Nwankpa, and M. Atzmon, Journal of Applied Physics **109**, 053522 (2011).
[8] J. Ding, S. Patinet, M. L. Falk, Y. Cheng, and E. Ma, Proceedings of the National Academy of Sciences **111**, 14052 (2014).
[9] K. E. Jensen, D. A. Weitz, and F. Spaepen, Physical Review E **90**, 042305 (2014).
[10] M. Atzmon and J. D. Ju, Phys. Rev. E **90**, 042313 (2014).
[11] J. Ju and M. Atzmon, Journal of Alloys and Compounds **643**, S8 (2015).
[12] W. Chen, Z. Liu, J. Ketkaew, R. M. O. Mota, S.-H. Kim, M. Power, W. Samela, and J. Schroers, Acta Materialia **107**, 220 (2016).
[13] J. Antonaglia, X. Xie, G. Schwarz, M. Wraith, J. Qiao, Y. Zhang, P. K. Liaw, J. T. Uhl, and K. A. Dahmen, Scientific Reports **4**, 4382 (2014).
[14] G. Kumar, P. Neibecker, Y. H. Liu, and J. Schroers, Nature Communications **4**, 1536 (2013).
[15] O. Gendelman, P. K. Jaiswal, I. Procaccia, B. S. Gupta, and J. Zylberg, Europhysics Letters **109**, 16002 (2015).
[16] K.-W. Park, C.-M. Lee, M. Wakeda, Y. Shibutani, M. L. Falk, and J.-C. Lee, Acta Materialia **56**, 5440 (2008).
[17] I. Regev, J. Weber, C. Reichhardt, K. A. Dahmen, and T. Lookman, Nature Communications **6**, 8805 (2015).
[18] J. S. Harmon, M. D. Demetriou, W. L. Johnson, and K. Samwer, Physical Review Letters **99**, 135502 (2007).
[19] T. Fujita, Z. Wang, Y. Liu, H. Sheng, W. Wang, and M. Chen, Acta Materialia **60**, 3741 (2012).
[20] W. Dmowski, T. Iwashita, C.-P. Chuang, J. Almer, and T. Egami, Physical Review Letters **105**, 205502 (2010).
[21] J. Ding, Y. Cheng, and E. Ma, Applied Physics Letters **101**, 121917 (2012).
[22] A. Argon and H. Kuo, Materials Science and Engineering **39**, 101 (1979).
[23] J. S. Langer, Physical Review E **77**, 021502 (2008).
[24] D. L. Malandro and D. J. Lacks, The Journal of Chemical Physics **110**, 4593 (1999).
[25] P. G. Debenedetti and F. H. Stillinger, Nature **410**, 259 (2001).
[26] G. Kumar, S. Prades-Rodel, A. Blatter, and J. Schroers, Scripta Materialia **65**, 585 (2011).
[27] J. Zemp, M. Celino, B. Schönfeld, and J. F. Löffler, Physical Review Letters **115**, 165501 (2015).
[28] J. Ashwin, E. Bouchbinder, and I. Procaccia, Physical Review E **87**, 042310 (2013).
[29] W. Kob and H. C. Andersen, Physical Review E **51**, 4626 (1995).
[30] M. P. Allen and D. J. Tildesley, *Computer simulation of liquids* (Oxford University Press, 1989).
[31] S. Plimpton, Journal of Computational Physics **117**, 1 (1995).
[32] M. E. Tuckerman, J. Alejandre, R. López-Rendón, A. L. Jochim, and G. J. Martyna, Journal of Physics A: Mathematical and General **39**, 5629 (2006).
[33] F. H. Stillinger, Science **267**, 1935 (1995).
[34] P. Charbonneau, J. Kurchan, G. Parisi, P. Urbani, and F. Zamponi, Nature Communications **5** (2014).
[35] D. J. Lacks and M. J. Osborne, Physical Review Letters

93, 255501 (2004).
[36] Y. Fan, T. Iwashita, and T. Egami, Nature Communications **5**, 5083 (2014).
[37] J. Lewandowski, W. Wang, and A. Greer, Philosophical Magazine Letters **85**, 77 (2005).
[38] H. B. Yu, X. Shen, Z. Wang, L. Gu, W. H. Wang, and H. Y. Bai, Physical Review Letters **108**, 015504 (2012).
[39] J. Schroers and W. L. Johnson, Physical Review Letters **93**, 255506 (2004).
[40] Y. Shi, J. Luo, F. Yuan, and L. Huang, Journal of Applied Physics **115**, 043528 (2014).
[41] A. Taub and F. Spaepen, Journal of Materials Science **16**, 3087 (1981).
[42] M. Kanik, P. Bordeenithikasem, G. Kumar, E. Kinser, and J. Schroers, Applied Physics Letters **105**, 131911 (2014).
[43] C. F. Schreck, R. S. Hoy, M. D. Shattuck, and C. S. OHern, Physical Review E **88**, 052205 (2013).
[44] I. Regev, T. Lookman, and C. Reichhardt, Physical Review E **88**, 062401 (2013).
[45] D. Fiocco, G. Foffi, and S. Sastry, Physical Review Letters **112**, 025702 (2014).
[46] N. V. Priezjev, Physical Review E **93**, 013001 (2016).